J Electr Eng Technol.2018; 13(5): 1945-1955
http://doi.org/10.5370/JEET.2018.13.5.1945

ISSN(Print) 1975-0102
ISSN(Online) 2093-7423

A Sensorless Rotor Position Estimation Scheme for IPMSM Using HF Signal Injection with Frequency and Amplitude Optimization

Jiadong Lu*, Jinglin Liu†, Yihua Hu, Xiaokang Zhang*, Kai Ni** and Jikai Si*****

Abstract – High frequency signal injection (HFI) is an alternative method for estimating rotor position of interior permanent magnet synchronous motor (IPMSM). The general method of frequency and amplitude selection is based on error tolerance and experiments, and is usually set with only one group of HF parameters, which is not efficient for different working modes. This paper proposes a novel rotor position estimation scheme by HFI with optimized frequency and amplitude, based on the mathematic model of IPMSM. The requirements for standstill and low-speed operational modes are met by applying this novel scheme. Additionally, the effects of the frequency and amplitude of the injected HF signal on the position estimation results under different operating conditions are analyzed. Furthermore, an optimization method for HF parameter selection is proposed to make the estimation process more efficient under different working conditions according to error tolerance. The effectiveness of the propose scheme is verified by the experiments on an IPMSM motor prototype.

Keywords: AC motor drives, HF parameter optimization, HF signal injection, Interior permanent magnet synchronous motor, Sensorless control.

1. Introduction

Interior permanent magnet synchronous motors (IPMSM) are now widely used in industrial fields, such as industrial robots, electric vehicles, high-end CNC (Computer Numerical Control) machine tools, etc., owing to their high energy density, fast dynamic response and strong overload capacity [1-4]. In order to achieve precise control of IPMSM, accurate information of the rotor position is required. The commonly used method is mounting a position sensor on the motor shaft end, such as encoder, resolver, holzer, etc., and a corresponding decoding circuit is designed to obtain the rotor position. However, it boosts the cost, and more importantly, the system reliability is reduced due to the addition of sensors, electronic devices and extra cabling. As an alternative, sensorless control technology can be used to improve the overall reliability of the system in case of position sensor failure. Therefore, sensorless control is mainly concerned and widely applied as a technology to eliminate the defects of traditional position sensors [5-8].

† Corresponding Author: School of Automation, Northwestern Polytechnical University, and Shaanxi Key Laboratory of Small & Special Electrical Machine and Drive Technology, Xi'an, China. (jinglinl@nwpu.edu.cn)
* School of Automation, Northwestern Polytechnical University, and Shaanxi Key Laboratory of Small & Special Electrical Machine and Drive Technology, Xi'an, China. (noodle@mail.nwpu.edu.cn)
** Dept. of Electrical Engineering and Electronics, University of Liverpool, Liverpool, U.K.
*** School of Electrical Engineering and Automation, Henan Polytechnic University, JiaoZuo, China.
Received: July 24, 2017 ; Accepted: April 24 2018

Two basic methods of estimating the rotor position are: mathematical model based method [2, 9-13] and magnetic saliency tracking based method [14-20]. The mathematical model based method has good performance at high speed. However, it gives the motor poor performance under low speed and standstill conditions, and its algorithm is usually complicated, which means the performance can be easily affected by the changes of motor parameters. Magnetic saliency tracking based method, such as high frequency signal injection (HFI) method, has good performance at standstill and low speed conditions, which makes it popular and widely applied. The HF signal can be sinusoidal-wave signal [15-17] or square-wave-type carrier signal [18-20].

For sinusoidal-wave signal injection based strategies, researchers have done a lot of work. In [21], a novel pulse width modulation (PWM) scheme for multi-space-vector pulse width modulation (MSVPWM) is proposed, which is used in position sensorless control of IPMSM drives. In [22], sensorless vector control operating under fault conditions is discussed. In [23], the influence of asymmetric machine parameters on carrier signal injection-based (rotating or pulsating) sensorless control of PMSMs is investigated. In [24], the HF inductance harmonics generated due to the saturation modulation between the HF field and main flux field are utilized for rotor position estimation. Paper [25] proposed a strategy to select an appropriate voltage amplitude for the injected HF signal for rotor position estimation. Significant electromagnetic and acoustic noises are caused when the fixed-frequency signal injection method is employed in conventional HF sensorless control

schemes for IPMSM drives [26]. The general method of selecting the values of frequency and amplitude for HF signals is based on error tolerance and experiments, and is usually set with only one group of HF parameters. This approach is usually effective, whereas it takes a lot of time and effort [27-29]. Moreover, from the following chapters of this paper it is found that the effects of the HF frequency and amplitude on position estimation are different under different operating conditions. In other words, the HF frequency and amplitude should be selected according to different motor running states. Smaller estimation error can be obtained by simply increasing the HF amplitude, whereas an excessive HF amplitude increases additional system losses and vibration. Besides, with the increase of amplitude, the decreasing rate in error becomes lower. In most of the cases, the selected value of HF frequency is much bigger than that of the fundamental frequency, whereas it is much smaller than that of the switching frequency [30, 31]. However, when the same error tolerance is applied, the value of HF frequency affects the selection of HF amplitude, and the specific reflection of the effects depends on the operating conditions. To meet the error tolerance, a sufficiently large HF amplitude should be set, whereas concerning the system efficiency and additional vibration, the magnitude cannot be set with an excessive big value. To satisfy the two requirements simultaneously, and take into account the different operating conditions, optimal HF parameters should be obtained.

Therefore, in this paper, the mathematic model of IPMSM is analyzed, and then, a novel IPMSM rotor position estimation method with HF amplitude and frequency optimization is proposed for standstill and low-speed conditions to meet the error tolerance and decrease the additional system losses and vibration with an appropriate value of HF amplitude. The paper indicates that the optimal HF frequency and amplitude should be selected according to different operating conditions and speed ranges to meet the estimation error tolerance. The structure of this paper is organized as follows. In the second part, a novel IPMSM rotor position estimation method is proposed. In the third part, the effects of HF frequency and amplitude on the position estimation error under different operating conditions are analyzed through experimental results on an IPMSM. In the fourth part, HF method with amplitude and frequency optimization is analyzed. In the fifth part, experimental results and analysis are illustrated. In the sixth part, the conclusion of this paper is given.

2. High Frequency Signal Injection (HFI) Method

The voltage and magnetic flux of the IPMSM in the Clark (α-β) reference are given by [21]

$$\begin{bmatrix} u_\alpha \\ u_\beta \end{bmatrix}=R\begin{bmatrix} i_\alpha \\ i_\beta \end{bmatrix}+\begin{bmatrix} L_0+L_2\cos 2\theta & L_2\sin 2\theta \\ L_2\sin 2\theta & L_0-L_2\cos 2\theta \end{bmatrix}\times\frac{d}{dt}\begin{bmatrix} i_\alpha \\ i_\beta \end{bmatrix} +\frac{d\theta}{dt}\left(2L_2\begin{bmatrix} -\sin 2\theta & \cos 2\theta \\ \cos 2\theta & \sin 2\theta \end{bmatrix}\begin{bmatrix} i_\alpha \\ i_\beta \end{bmatrix}+\psi_f\begin{bmatrix} -\sin\theta \\ \cos\theta \end{bmatrix}\right) \tag{1}$$

$$L_0=\left(L_d+L_q \right)/2 \tag{2}$$

$$L_2=\left(L_d\text{-}L_q \right)/2 \tag{3}$$

$$\begin{cases} L_0>0>L_2 \\ |L_0|>|L_2| \end{cases}. \tag{4}$$

In (1), ω and R can be ignored when analyzing the HF currents. Thus HF voltage of IPMSM can be obtained from (1) ~ (4) by ignoring the first and third items in (1)

$$\begin{bmatrix} u_{\alpha h} \\ u_{\beta h} \end{bmatrix}=\begin{bmatrix} L_0+L_2\cos(2\theta) & L_2\sin(2\theta) \\ L_2\sin(2\theta) & L_0-L_2\cos(2\theta) \end{bmatrix}\cdot\frac{d}{dt}\begin{bmatrix} i_{\alpha h} \\ i_{\beta h} \end{bmatrix}. \tag{5}$$

The HF signals are given by

$$\begin{bmatrix} u_{\alpha h} \\ u_{\beta h} \end{bmatrix}=\sqrt{\frac{2}{3}}U_h\begin{bmatrix} \cos(\omega_h t) \\ \sin(\omega_h t) \end{bmatrix}. \tag{6}$$

Combining (5), (6), and 2/3 transformation, the HF current response (in three phase static reference frame) are given by

$$\begin{bmatrix} i_{Ah} \\ i_{Bh} \\ i_{Ch} \end{bmatrix}=k\left\{ L_0\cdot\begin{bmatrix} \sin(\omega_h t) \\ \sin(\omega_h t-2\pi/3) \\ \sin(\omega_h t+2\pi/3) \end{bmatrix} -L_2\cdot\begin{bmatrix} \sin(\omega_h t-2\theta) \\ \sin(\omega_h t-2\theta+2\pi/3) \\ \sin(\omega_h t-2\theta-2\pi/3) \end{bmatrix}\right\} \tag{7}$$

$$k=U_h/\left[\omega_h\left(L_0^2-L_2^2 \right)\right]>0. \tag{8}$$

From (7) and (8), it is known that the phase difference between the positive and negative sequence components in (7) is related to the rotor position which is given by

$$\begin{cases} \varphi_A^+=\omega_h t \\ \varphi_A^-=\omega_h t-2\theta \end{cases} \tag{9}$$

$$\begin{cases} \varphi_B^+=\omega_h t-2\pi/3 \\ \varphi_B^-=\omega_h t-2\theta+2\pi/3 \end{cases} \tag{10}$$

$$\begin{cases} \varphi_C^+=\omega_h t+2\pi/3 \\ \varphi_C^-=\omega_h t-2\theta-2\pi/3 \end{cases}. \tag{11}$$

Therefore, by separating the positive and negative sequence components, the phase of each component can be obtained by least square fitting, and finally the rotor position can be obtained by calculating the phase difference:

1) The phase difference between the positive and negative sequence components in phase A is two times of θ

$$\theta=\left(\varphi_A^+-\varphi_A^-\right)/2. \tag{12}$$

2) The phase difference between the positive and negative sequence components in phase B minus $2\pi/3$ is two times of θ

$$\theta=\left(\varphi_B^+-\varphi_B^--2\pi/3\right)/2. \tag{13}$$

3) The phase difference between the positive and negative sequence components in phase C plus $2\pi/3$ is two times of θ

$$\theta=\left(\varphi_C^+-\varphi_C^-+2\pi/3\right)/2. \tag{14}$$

4) Summation of the phase differences between the positive and negative sequence components in phase A, B, and C is six times of θ

$$\theta=\left[\left(\varphi_A^+-\varphi_A^-\right)+\left(\varphi_B^+-\varphi_B^-\right)+\left(\varphi_C^+-\varphi_C^-\right)\right]/6. \tag{15}$$

Any of the above methods can be used to estimate the rotor position. Taking into account the actual application of the software overhead, the rotor position can be estimated by analyzing the positive and negative sequence components of an arbitrary phase. The experimental results show that the rotor position can be estimated by any of the 4 methods mentioned above, and there are no obvious differences among the estimated values. The rotor position estimation in the following parts in this paper is obtained by analyzing the HF current response of phase A.

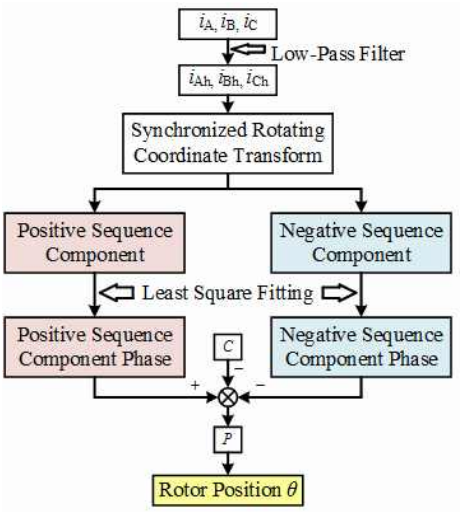

Fig. 1. Structure diagram of rotor position estimation method

The proposed position estimation process flow chart is shown in Fig. 1, where C and P represent coefficients of different estimation methods. The three-phase HF currents are firstly obtained by band pass filtering (BPF) of the phase currents. The synchronized rotating coordinate transform is utilized to calculate the positive and negative sequence components of HF currents. And then least square fitting algorithm is applied in the phase angle extraction process which are used in (12) to obtain rotor position. The rotor velocity can be calculated as the low-pass filtering of the differential value of rotor position

$$\omega(k)=K\cdot\omega(k-1)+(1-K)\cdot\frac{\pi\cdot\left[\theta(k)-\theta(k-1)\right]}{180\cdot\Delta t}. \tag{16}$$

3. Effects of the HF Frequency and Amplitude on Position Estimation Results

In this paper, experiments have been carried out on an IPMSM motor prototype using the proposed sensorless control technique to analyze the effects of the HF frequency and amplitude on the position estimation error under different operating conditions.

In the following parts, estimation results have been studied in detail with different HF frequencies and amplitudes under the five operating conditions (including starting operation, low speed operation, mid-low speed operation, medium speed operation and speed reverse operation).

An experimental platform with an 11kW IPMSM motor prototype shown in Fig. 2 is used to verify the effectiveness of the propose scheme. Table 1 lists the parameters of the IPMSM. A magnetic powder brake is coaxially connected to the IPMSM to set up the test load. The controller is supplied to IPMSM in AC-DC-AC mode, and the control algorithm is realized by a DSP chip TMS320F2812 produced by TI. The PWM frequency is set to 10kHz, which is realized by an intelligent power module (IPM) PM75RLA120 (produced by Mitsubishi).

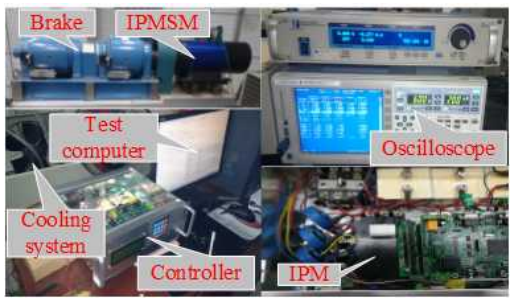

Fig. 2. Experimental platform

Table 1. Motor prototype parameters

Parameter	VALUE	Parameter	Value
Rated power	11 kW	Rated toque	17.5 Nm
Rated speed	6000 r/min	Resistance	0.18 Ω
Rated voltage	380 V	*d*-axis Inductance	4.2 mH
Rated current	16.7 A	*q*-axis Inductance	10.1 mH

Table 2. Average estimation error in starting mode Δθ(°)

U_h(V) \ f_h(Hz)	500	750	1000	1250	1500
10	4.02	5.83	6.1	6.49	7.02
20	3.21	3.4	3.61	3.95	4.55
30	2.68	2.73	2.86	3.62	3.5
40	2.6	2.65	2.81	3.14	3.15
50	2.57	2.54	2.63	2.6	2.96
60	2.51	2.53	2.55	2.57	2.86
70	2.32	2.45	2.39	2.44	2.75
80	2.15	2.33	2.28	2.36	2.71

The HF frequency is set to 500Hz, 750Hz, 1000Hz, 1250Hz, 1500Hz, and the amplitude is set to 10V, 20V, ..., 80V for each operating mode, in order to obtain the estimation result from low to extremely high accuracy. Estimation results are different under diverse HF frequencies and amplitudes. Actual and estimated rotor positions with estimation errors by applying various combination of HF frequencies and amplitudes are presented in Fig. 3 respectively for the five operating modes. In addition, the most and least accurate estimation waveforms are displayed.

3.1 Starting mode operation

Starting operation refers to the process of starting a motor from the static state. In this paper, the speed of the motor is set from 0 rpm to 150 rpm for this mode.

More accurate position estimation results are derived based on the extreme selection of the HF frequency and amplitude, which brings more noise and vibration, deteriorating the efficiency of the system. The maximum position estimation error in the starting mode decreases with the increase of HF amplitude in each frequency band, among which the estimation in the low frequency segment is more accurate. Numerical data of the average estimation error are shown in Table 2, in which the minimum estimation error occurs in the case of 80 V, 500 Hz.

3.2 Low speed operation

Low speed operation refers to the motor running at a very low speed, which is selected as 100rpm in the experiment.

Similar to the previous mode, the accuracy of the rotor position estimation is increased when the amplitude of the injected HF signal goes higher in each frequency band. On the contrary, an inaccurate estimation is obtained in the case of 10 V, 1500 Hz. In general, estimation in low frequency bands gives small error. Numerical data of the average estimated error are shown in Table 3, where the minimum estimation error occurs in the case of 80 V, 1000 Hz.

Table 3. Average estimation error in low speed operation Δθ(°)

U_h(V) \ f_h(Hz)	500	750	1000	1250	1500
10	4.17	5.26	6.34	7.25	29.11
20	2.856	3.73	4.57	4.77	5.65
30	2.15	2.76	3.5	3.67	4
40	1.86	2	2.66	3.11	3.23
50	1.64	1.69	1.85	2.71	2.94
60	1.64	1.67	1.82	2.47	2.92
70	1.64	1.6	1.73	2.32	2.65
80	1.6	1.56	1.43	2.07	2.30

Table 4. Average estimation error in mid-low speed operation Δθ(°)

U_h(V) \ f_h(Hz)	500	750	1000	1250	1500
10	4.68	5.1	6.04	7.43	76.46
20	2.59	3.2	4.35	4.37	5.04
30	2.04	2.52	3.52	3.59	4.31
40	1.91	2.23	2.86	3.4	4.03
50	1.76	1.97	2.58	2.86	3.27
60	1.75	1.8	2.16	2.56	3.09
70	1.7	1.67	1.75	2.13	2.62
80	1.69	1.6	1.52	1.79	2.18

3.3 Mid-low speed operation

Mid-Low speed operation is explained as the state when the motor is running at a speed which is a little bit larger than that of the low speed operation. In this paper, the speed of the motor in this operational mode is set to 300 rpm.

From Fig. 3(c), it can be seen that the maximum position estimation error in mid-low speed mode decreases with the increase of HF amplitude in each frequency band. More accurate estimation is derived in the low frequency segment. In addition, the position estimation fails in the case of 10 V, 1250/1500 Hz. Numerical data of the average estimated error are shown in Table 4, and when the amplitude and frequency are set to 80 V, 1000 Hz, the estimation is the most accurate.

3.4 Medium speed operation

When the motor runs at a moderate speed, the operational mode is defined as medium speed operation. For this operational state, the speed of the motor is set to 800 rpm.

An inverse proportional relationship between the maximum position estimation error in the medium speed mode and the HF amplitude in each frequency band is observed, among which the estimation for the middle frequency segment is more accurate. In the cases of 10 V, 500/750/1500 Hz, failure in estimating the rotor position

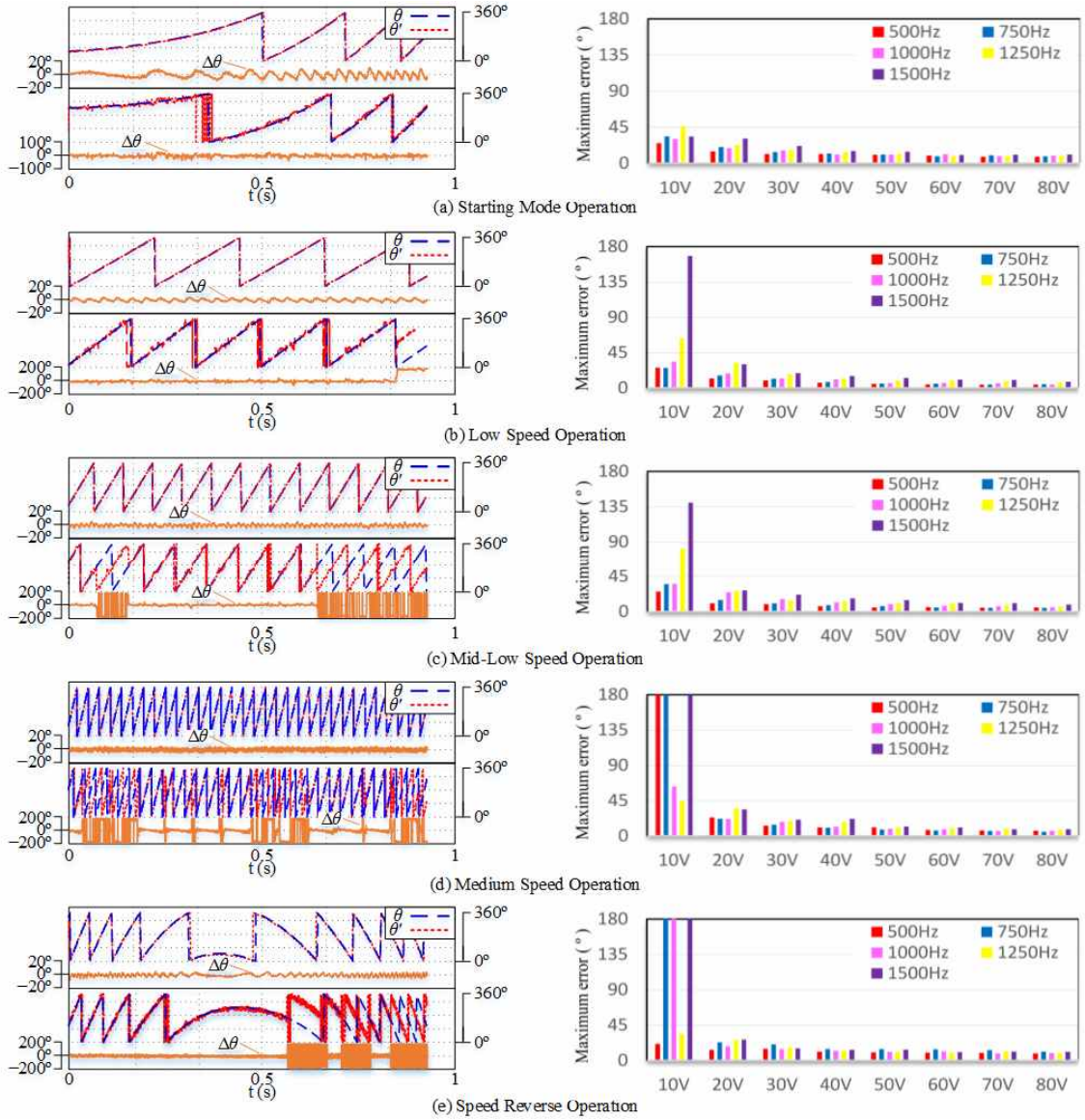

Fig. 3. Actual and estimated rotor position with estimation error, maximum estimated rotor position error in different HF parameters and operating conditions

Table 5. Average estimation error in medium speed operation Δθ(°)

U_h(V) \ f_h(Hz)	500	750	1000	1250	1500
10	82.7	94.76	7.62	6.92	94.95
20	5.71	4.63	5.17	5.3	5.65
30	4.04	3.42	3.78	3.91	4.27
40	3.09	2.62	3.01	3.33	3.62
50	2.5	2.09	2.56	2.68	3.11
60	2.15	1.87	2.18	2.47	2.86
70	2.01	1.75	1.85	2.22	2.51
80	1.91	1.62	1.73	2.11	2.31

appears. According to numerical data of the average estimated error displayed in Table 5, the case of 80 V, 750 Hz gives the minimum estimation error.

3.5 Speed reverse operation

Different from all the four modes mentioned above, the rotating direction of the motor for speed reverse operation changes during the process. In this paper, the motor speed is set from 400 rpm to -400 rpm.

When the HF amplitude in each frequency band rises, the maximum position estimation error in the speed reverse condition is reduced. In terms of the erroneous position estimation situations, 10 V, 750/1000/1500 Hz are selected as the amplitude and frequencies respectively. Referring to Table 6, the minimum estimation is obtained when the case of 80 V, 500 Hz is selected, which gives the most accurate estimation.

Taking the motor in this paper for an example, if the error tolerance is set as $\Delta\theta \leqq 3°$(electric angle), HF

Table 6. Average estimation error in speed reverse operation Δθ(°)

U_h(V) \ f_h(Hz)	500	750	1000	1250	1500
10	4.63	59.59	22.11	6.32	8.82
20	3.31	6.47	3.99	4.23	4.58
30	3.11	4.61	3.43	3.45	3.68
40	3.02	3.77	3.09	3.11	3.63
50	2.76	3.55	2.83	2.68	3.37
60	2.69	3.33	2.7	2.65	2.8
70	2.64	2.79	2.63	2.58	2.74
80	2.58	2.69	2.55	2.53	2.61

frequency and amplitude combination that meet the requirements are those with grey shading marks in Table 2~6. Considering the efficiency, vibration and noise, smaller HF amplitudes are better choices. Besides, a lower HF frequency produces more vibration and noise. Thus efficiency, vibration and noise should be considered when selecting the optimal combination of the amplitude and frequency for the HF signal. Optimal combination in Table 2 ~ 6 are those marked with a box ($\Delta\theta \leqq 3^{\circ}$). It can be seen that the optimal HF signal combinations are not exactly the same under different operating conditions.

4. Effects of the HF Frequency and Amplitude on Position Estimation Results

4.1 Principle of amplitude and frequency optimization

From (7) and (8), it is clear that three phase HF current responses are sinusoidal waveforms with variable amplitudes. Because θ is extracted from the HF current signal, in order to increase estimation accuracy, proper HF parameters should be obtained. If the signal-to-noise ratio is lower than a reasonable value, a large estimation error will be derived. By combining (3), (7), and (8), the range of variation for three phase HF current amplitude is given by

$$\begin{cases} I_{peak\max} = k \cdot (L_0 - L_2) = U_h / (\omega_h L_d) > 0 \\ I_{peak\min} = k \cdot (L_0 + L_2) = U_h / (\omega_h L_q) > 0 \end{cases}. \quad (17)$$

Apparently, the maximum/minimum peak value of HF current depends linearly on the value of the injected HF voltage value U_h, and inversely proportional to the HF signal electrical angular velocity ω_h. In addition, the peak value varies due to the different d-q axis inductance. To obtain a lower estimation error, U_h can be set with a relatively high value if necessary, however, f_h cannot be set too low to avoid the noise generated by model approximation (shown in (5)) and frequency interference. As f_h is about median of the fundamental frequency f_f and switching frequency f_s, as shown in (18), it is very susceptible to interference. In addition, due to the presence of system white noise, the interference can be very serious from time to time. In order to obtain the optimal system efficiency and meet the requirements of estimation accuracy, the optimized values of U_h and f_h should be obtained.

$$f_f < f_h < f_s \quad (18)$$

From the above analysis, it can be seen that under each operating condition, a large error or even failure may occur in the estimation process by injecting a HF signal with a very small amplitude. Smaller position estimation error can be obtained by increasing the HF amplitude, whereas an excessive HF amplitude increases the system losses, producing more vibration and noise, and the decline in error decelerates with the increase of amplitude. Therefore, it is very important to select a reasonable value for the HF amplitude. HF frequencies also cause some impacts on the estimation results: in low speed conditions, it is clear that lower HF frequencies lead to more accurate estimation results; whereas in the medium speed or speed reverse conditions, the optimal frequency of the HF signal tends to have a larger value. From another point of considering this problem, in the case of the same error tolerance, the minimum value of the HF amplitude varies with different HF frequencies, i.e., an appropriate value of HF frequency minimizes the HF amplitude. Even if the selections of the HF frequency and amplitude are totally the same for different operating conditions, there are distinct differences among the estimation errors. Under this circumstance, in order to get better estimation results in practical applications, it is necessary to optimize values of HF frequency and amplitude according to different operating conditions and speed segments. If one group of HF frequency and amplitude is set, an accurate estimation

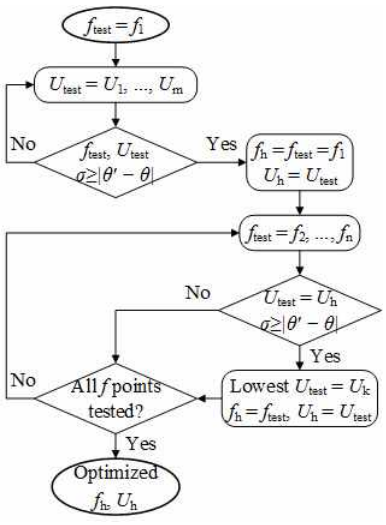

Fig. 4. Flow chart of rotor position estimation method

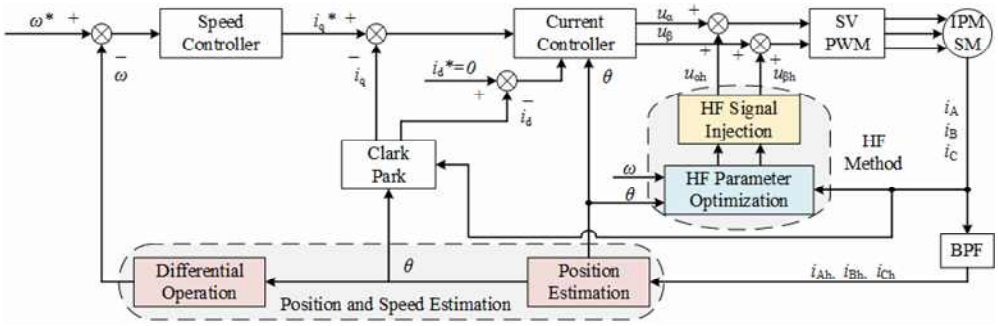

Fig. 5. Structure diagram of IPMSM drive using HFI scheme with amplitude and frequency optimization

of the rotor position is likely to be obtained. However, such an accurate estimation is not necessary in some cases, whereas the accuracy does not meet the requirements in other cases.

4.2 Optimized parameter selection method

HF parameters should be optimized according to operating conditions and estimation error tolerance. In order to obtain the optimal HF parameters by a minimum number of trials, a few steps should be carried out as shown in Fig. 4.

1) An average error tolerance σ should be chosen first, which is based on the comparison with the difference between the estimated rotor angle and the actual one.

$$\sigma \geq \left| \theta' - \theta \right|. \tag{19}$$

Then, a series of discrete HF frequency testing points f_1, f_2, ..., f_n, that meet the requirements of (18), and HF amplitude testing points U_1, U_2, ..., U_m are selected

$$\begin{cases} f_1 < f_2 < \cdots < f_n \\ U_1 < U_2 < \cdots < U_m \end{cases}. \tag{20}$$

2) Select different operating conditions for tests. From U_1 to U_m, test if the estimation error meets (19) by using $f_{test} = f_1$. Once (19) is satisfied by U_k, U_h, and f_h is defined by (21), the next frequency point will be tested

$$\begin{cases} U_h = U_k \\ f_h = f_{test} \end{cases}. \tag{21}$$

3) By applying $f_{test} = f_2$, ..., f_n, test if U_h satisfies (19). If not, test the next frequency point without changing U_h and f_h. Otherwise, the lowest HF amplitude U_k with the frequency f_{test} which satisfies (19), should be tested by applying values from U_h to U_1, then U_h and f_h will be redefined by (21), after that the next frequency point will be tested. Finally, the optimal HF parameters are obtained.

In this part, the HF parameters optimization method for a specified operating mode is illustrated. The selected HF parameters reach the optimal control results in the specified operating mode. Whereas for other operation conditions, the control results using the selected HF parameters may not meet the control requirements. For different working conditions in this paper, the optimized HF parameters are selected from the previously tested parameters for each operating mode.

A structure diagram of IPMSM drive using the HFI scheme with amplitude and frequency optimization is shown in Fig. 5. The two pink blocks are position and speed estimation processes using HF method. The yellow block represents the HF signal injection process. The HF parameter optimizing process is illustrated by the cyan block, which judges the motor running state by analyzing the estimated motor speed, rotor position and winding current, and then the optimized HF amplitude and frequency are given.

5. Experimental Results and Analysis

Fig. 6 illustrates the experimental results of phase currents and d-q axis currents between single group of HF signal (750Hz, 30V, scheme 1 with subscript "1") and different HF signal combinations (scheme 2 with subscript "2"). From 0 s to 0.75 s the motor operates at starting mode. From 0.75 s to 1.05 s the motor operates at very low speed of 100 rpm. From 1.05 s to 1.35 s the motor operates at medium speed of 300 rpm. From 1.35 s to 1.95 s the motor operates a speed reversing mode from 300 rpm to -800 rpm. From 2.2 s to 2.5 s the motor operates at high speed of -800 rpm. The experimental results of rotor speed and position are displayed in Fig. 7. From the figure, it can be seen that the two schemes meet the needs of position estimation under different operating conditions. In the figure, the experimental results of scheme 1 have relatively small errors in both starting and low speed operations, whereas the difference of results between the two schemes is not distinct. However, in high speed and speed reverse operations, the situation is completely different, where the error in the estimated value in scheme 1 is much larger than that in scheme 2. By applying variable HF parameters, improvements are shown in high speed and speed reverse operations compared to scheme 1. Estimation error in

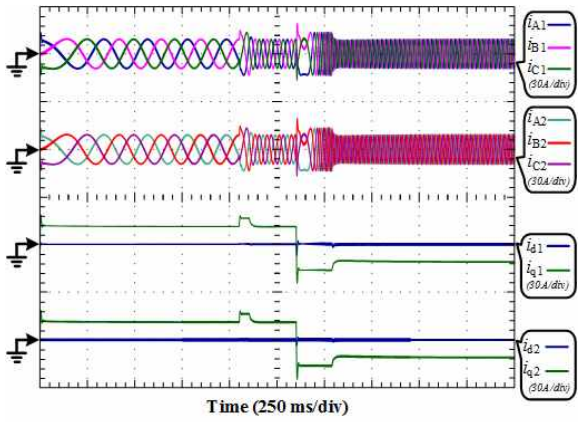

Fig. 6. Experimental results of phase currents and d-q axis currents between single group of HF signal (750Hz, 30V) and different HF signal combinations

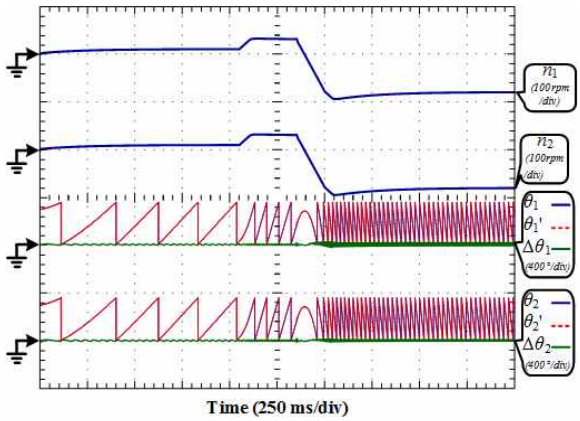

Fig. 7. Experimental results of rotor speed and position between single group of HF signal (750Hz, 30V) and different HF signal combinations

Table 7. Comparison between HF method and parameter optimized method

	HF method using one group of HF parameter	Parameter optimization method
HF parameters	Remain the same.	Vary with operating conditions.
Estimation results	Vary with operating conditions.	Gain same estimation result.
Estimation Efficiency	Vary with operating conditions due to a constant HF amplitude.	Gain same efficiency due to a variable HF amplitude.
System losses, vibration and noise	Increased due to excessive HF amplitude, which is not necessary in some conditions.	Reduced by applying variable HF amplitude.
Algorithm	Simple.	Slightly complex.

scheme 2 remain approximately unchanged during different operations. It can be concluded that estimation results of scheme 1 which utilizes single parameter of HF signal (750 Hz, 30 V), have better estimation results in starting and low speed operations. Whereas from about 1.05 s when the motor operates medium or high speed and reversing modes, the estimation error become larger. By applying variable HF parameters, the estimation error in all operation modes can be controlled within a same low level. In addition, vibration and noise is also reduced in starting and low speed operations by depressing the HF magnitude, because such high HF magnitude is unnecessary in scheme 1. Estimation error, as depicted in Fig. 7, still exists even in HF parameter optimized method. Which is mainly caused by current sampling error, external disturbance, model mathematical approximation error, asymmetry of the motor structure and the current response error caused by different saturation of the rotor.

Comparison between the HF method mentioned in [15, 16, 25, 28] (using one group of HF parameter) and the proposed parameter optimization method in the fourth part (using different HF parameters according to operating conditions) are shown in Table 7. From Table 7, it can be seen that HF parameters in the optimized method vary with operating states compared to the method using one group of HF parameter. In the optimized method, no significant differences in estimation results are displayed under different operating conditions compared to the other method. Additionally, under certain operating conditions, the system losses, vibration and noise are reduced due to the decrease in the HF amplitude.

6. Conclusion

In this paper a novel HF method was proposed for sensorless control of IPMSM by using a HF amplitude and frequency optimization scheme. Firstly, the mathematical model of IPMSM was derived by reasonable analysis. Secondly, a sensorless rotor position estimation scheme was proposed for IPMSM using HF signal injection with frequency and amplitude optimization. It was deduced that the increase of HF amplitude contributed to more accurate estimation results, whereas some problems occurred, such as increased vibration, noise and losses. Thirdly, corresponding analysis indicated that the value of the HF amplitude varies with different HF frequencies when the same error tolerance was applied, and a more reasonable choice of HF frequency reduced the HF amplitude. The optimal HF parameters were selected according to different operating states and speed ranges to obtain a more accurate estimation result. Finally, an HF parameter optimization method was proposed and the comparison with the method using one group of HF parameter was given.

Nomenclature

u_α, u_β, i_α, i_β Voltages and currents in the Clark (α-β) reference frame.

$u_{\alpha h}$, $u_{\beta h}$, $i_{\alpha h}$, $i_{\beta h}$ HF voltages and currents in the Clark reference frame.

u_{Ah}, u_{Bh}, u_{Ch} HF signal voltage in three phase static

(A-B-C) frame (V).

i_{Ah}, i_{Bh}, i_{Ch} HF current response in three phase static frame (A).

$I_{peakmax}$, $I_{peakmin}$ Maximum/minimum peak value of three phase HF current.

U_h HF signal voltage amplitude (V).

R Stator resistance (Ω).

d / d t Differential of time t.

ψ_f Full flux linkage of PM (Wb).

ω Electrical rotor speed (rad/s).

ω_h HF signal electrical angular velocity (rad/s).

f_h HF signal frequency (Hz).

θ, θ' Actual and estimated electrical rotor position (°).

$\Delta\theta$ Estimation error (°).

L_d, L_q d and q-axis stator inductances (H).

φ_A^+, φ_B^+, φ_C^+ Positive sequence component phases.

φ_A^-, φ_B^-, φ_C^- Negative sequence component phases.

Acknowledgement

This work was supported by Shaanxi Science Technology Co-ordination and Innovation Project, China (2013KTCQ01-20, 2016KTCQ01-49)

References

[1] J. D. Lu, X. K. Zhang, Y. H. Hu, J. L. Liu, C. Gan, and Z. Wang, "Independent phase current reconstruction strategy for IPMSM sensorless control without using null switching states," *IEEE Trans. Ind. Electron.,* vol. 65, no. 6, pp. 4492-4502, June 2018.

[2] X. G. Zhang, and Z. X. Li, "Sliding-mode observer-based mechanical parameter estimation for permanent magnet synchronous motor," *IEEE Trans. Power Electron.*, vol. 31, no. 8, pp. 5732-5745, Aug. 2016.

[3] R. Z. Haddad, and E. G. Strangas, "On the accuracy of fault detection and separation in permanent magnet synchronous machines using MCSA/MVSA and LDA," *IEEE Trans. Energy Convers.*, vol. 31, no. 3, pp. 924-934, Sep. 2016.

[4] Q. An, J. Liu, Z. Peng, L. Sun, and L. Z. Sun, "Dual-space vector control of open-end winding permanent magnet synchronous motor drive fed by dual inverter," *IEEE Trans. Power Electron.*, vol. 31, no. 12, pp. 8329-8342, Dec. 2016.

[5] Y. Sangsefidi, S. Ziaeinejad, and A. M. Sani, "Sensorless speed control of synchronous motors: analysis and mitigation of stator resistance error," *IEEE Trans. Energy Convers.*, vol. 31, no. 2, pp. 540-548, Jun. 2016.

[6] P. L. Xu, and Z. Q. Zhu, "Novel carrier signal injection method using zero-sequence voltage for sensorless control of PMSM drives," *IEEE Trans. Ind. Electron.*, vol. 63, no. 4, pp. 2053-2061, Apr. 2016.

[7] B. C. Du, S. P. Wu, S. L. Han, and S. M. Cui, "Application of linear active disturbance rejection controller for sensorless control of internal permanent-magnet synchronous motor," *IEEE Trans. Ind. Electron.*, vol. 63, no. 5, pp. 3019-3027, May 2016.

[8] Y. C. Chang, C. H. Chen, Z. C. Zhu, and Y. W. Huang, "Speed control of the surface-mounted permanent-magnet synchronous motor based on takagi-sugeno fuzzy models," *IEEE Trans. Power Electron.*, vol. 31, no. 9, pp. 6504-6510, Sep. 2016.

[9] X. D. Song, J. C. Fang, B. C. Han, and S. Q. Zheng, "Adaptive compensation method for high-speed surface PMSM sensorless drives of EMF-based position estimation error," *IEEE Trans. Power Electron.*, vol. 31, no. 2, pp. 1438-1449, Feb. 2016.

[10] Y. Zhao, Z. Zhang, W. Qiao, and L. Wu, "An extended flux model-based rotor position estimator for sensorless control of salient-pole permanent-magnet synchronous machines," *IEEE Trans. Power Electron.*, vol. 30, no. 8, pp. 4412-4422, Aug. 2015.

[11] T. N. Shi, Z. Wang, and C. L. Xia, "Speed measurement error suppression for PMSM control system using self-adaption kalman observer," *IEEE Trans. Ind. Electron.*, vol. 62, no. 5, pp. 2753-2763, May 2015.

[12] N. K. Quang, N. T. Hieu, and Q. P. Ha, "FPGA-based sensorless PMSM speed control using reduced-order extended kalman filters," *IEEE Trans. Ind. Electron.*, vol. 61, no. 12, pp. 6574-6582, Dec. 2014.

[13] K. Y. Lu, X. Lei, and F. Blaabjerg, "Artificial inductance concept to compensate nonlinear inductance effects in the back EMF-based sensorless control method for PMSM," *IEEE Trans. Energy Convers.*, vol. 28, no. 3, pp. 593-600, Sep. 2013.

[14] J. D. Lu, Y. H. Hu, X. K. Zhang, Z. Wang, J. L. Liu, and C. Gan, "High frequency voltage injection sensorless control technique for IPMSMs fed by a three-phase four-switch inverter with a single current sensor," *IEEE/ASME Trans. Mechatronics*, vol. 23, no. 2, pp. 758-768, April, 2018.

[15] D. D. Reigosa, D. Fernandez, Z. Q. Zhu, and F. Briz, "PMSM magnetization state estimation based on stator-reflected PM resistance using high-frequency signal injection," *IEEE Trans. Ind. Appl.*, vol. 51, no. 5, pp. 3800-3810, Sep./Oct. 2015.

[16] G. Xie, K. Y. Lu, S. K. Dwivedi, R. J. Riber, and W. M. Wu, "Permanent magnet flux online estimation based on zero-voltage vector injection method," *IEEE Trans. Power Electron.*, vol. 30, no. 12, pp. 6506-6509, Dec. 2015.

[17] M. Seilmeier, and B. Piepenbreier, "Sensorless control of PMSM for the whole speed range using two-degree-of-freedom current control and HF test current injection for low-speed range," *IEEE Trans. Power Electron.*, vol. 30, no. 8, pp. 4394-4403, Aug.

2015.
[18] P. L. Xu, and Z. Q. Zhu, "Novel square-wave signal injection method using zero-sequence voltage for sensorless control of PMSM drives," *IEEE Trans. Ind. Electron.*, vol. 63, no. 12, pp. 7444-7454, Dec. 2016.
[19] Y. D. Yoon, S. K. Sul, S. Morimoto, and K. Ide, "High-bandwidth sensorless algorithm for ac machines based on square-wave-type voltage injection," *IEEE Trans. Ind. Appl.*, vol. 47, no. 3, pp. 1361-1370, May/Jun. 2011.
[20] J. M. Liu, and Z. Q. Zhu, "Sensorless control strategy by square-waveform high-frequency pulsating signal injection into stationary reference frame," *IEEE J. Emerg. Sel. Topics Power Electron.*, vol. 2, no. 2, pp. 171-180, Jun. 2014.
[21] M. Gu , S. Ogasawara, and M. Takemoto, "Novel PWM schemes with multi SVPWM of sensorless IPMSM drives for reducing current ripple," *IEEE Trans. Power Electron.*, vol. 31, no. 9, pp. 6461-6475, Sep. 2016.
[22] A. Gaeta, G. Scelba, and A. Consoli, "Sensorless vector control of PM synchronous motors during single-phase open-circuit faulted conditions," *IEEE Trans. Ind. Appl.*, vol. 48, no. 6, pp. 1968-1979, Nov./Dec. 2012.
[23] P. L. Xu, and Z. Q. Zhu, "Carrier signal injection-based sensorless control for permanent-magnet synchronous machine drives considering machine parameter asymmetry," *IEEE Trans. Ind. Electron.*, vol. 63, no. 5, pp. 2813-2824, May 2016.
[24] P. L. Xu, Z. Q. Zhu, and D. Wu, "Carrier signal injection-based sensorless control of permanent magnet synchronous machines without the need of magnetic polarity identification," *IEEE Trans. Ind. Appl.*, vol. 52, no. 5, pp. 3916-3926, Sep./Oct. 2016.
[25] S. Medjmadj, D. Diallo, M. Mostefai, C. Delpha, and A. Arias, "PMSM drive position estimation: contribution to the high-frequency injection voltage selection issue," *IEEE Trans. Energy Convers.*, vol. 30, no. 1, pp. 349-358, Mar. 2015.
[26] G. L. Wang, L. Yang, G. Q. Zhang, and D. G. Xu, "Comparative investigation of pseudorandom high-frequency signal injection schemes for sensorless IPMSM drives," *IEEE Trans. Power Electron.*, vol. 32, no. 3, pp. 2123-2132, Mar. 2017.
[27] M. Seilmeier, S. Ebersberger, and B. Piepenbreier, "HF test current injection-based self-sensing control of PMSM for low- and zero-speed range using two-degree-of-freedom current control," *IEEE Trans. Ind. Appl.*, vol. 51, no. 3, pp. 2268-2278, May/Jun. 2015.
[28] G. Xie, K. Y. Lu, S. K. Dwivedi, J. R. Rosholm, and F. Blaabjerg, "Minimum-voltage vector injection method for sensorless control of PMSM for low-speed operations," *IEEE Trans. Power Electron.*, vol. 31, no. 2, pp. 1785-1794, Feb. 2016.
[29] K. Liu, and Z. Q. Zhu, "Position-offset-based parameter estimation using the adaline NN for condition monitoring of permanent-magnet synchronous machines," *IEEE Trans. Ind. Electron.*, vol. 62, no. 4, pp. 2372-2383, Apr. 2015.
[30] T. Szalai, G. Berger, and J. Petzoldt, "Stabilizing sensorless control down to zero speed by using the high-frequency current amplitude," *IEEE Trans. Power Electron.*, vol. 29, no. 7, pp. 3646-3656, Jul. 2014.
[31] G. L. Wang, R. F. Yang, and D. G. Xu, "DSP-based control of sensorless IPMSM drives for wide-speed-range operation," *IEEE Trans. Ind. Electron.*, vol. 60, no. 2, pp. 720-727, Feb. 2013.

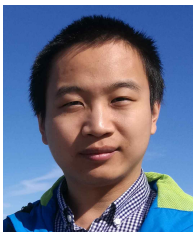

Jiadong Lu was born in Pucheng, China, in 1990. He received the B.S. and M.S. degrees in electrical engineering, in 2012 and 2015, respectively, from Northwestern Polytechnical University, Xi'an, China, where he is currently working toward the Ph.D. degree in electrical engineering. In 2017, he was with the Department of Electrical Engineering and Electronics, University of Liverpool, as a Research Assistant. His research interests include sensorless control and hybrid fault-tolerant control techniques for permanent magnet synchronous motor drives.

Jinglin Liu (M'01) received the B.Eng. degree in electrical engineering from Tsinghua University, Beijing, China, in 1986, and the M.Eng. and the Ph.D. degrees in electrical engineering from Northwestern Polytechnical University, Xi'an, China, in 1990 and 2002, respecttively. Since 1994, he has been a Faculty Member with Northwestern Polytechnical University, Xi'an, where he is currently a Professor of Electrical Engineering. His research interests include electrical machines design and drives, power electronics, fault diagnosis, and motion control.

Yihua Hu (M'13-SM'15) received the B.S. degree in electrical motor drives in 2003, and the Ph.D. degree in power electronics and drives in 2011, both from China University of Mining and Technology, Jiangsu, China. Between 2011 and 2013, he was with the College of Electrical Engineering, Zhejiang University as a Postdoctoral Fellow. Between November 2012 and February 2013, he was an academic visiting scholar with the School of Electrical and

Electronic Engineering, Newcastle University, Newcastle upon Tyne, UK. Between 2013 and 2015, he worked as a Research Associate at the power electronics and motor drive group, the University of Strathclyde. Currently, he is a Lecturer at the Department of Electrical Engineering and Electronics, University of Liverpool (UoL). He has published more than 50 peer reviewed technical papers in leading journals. His research interests include PV generation system, power electronics converters & control, and electrical motor drives.

Xiaokang Zhang was born in Zhejiang, China, in 1992. He received the B.S degree in electrical engineering from Northeast Agricultural University, Harbin, China, in 2015 and he is currently working toward the M.S degree in electrical engineering in Northwestern Polytechnical University. His research interests include sensorless control for permanent magnet synchronous motor and fault tolerant control techniques for motor drives.

Kai Ni was born in Jiangsu, China. He received the B.Eng degree in Electrical Engineering in 2016 from University of Liverpool, Liverpool, UK. He is currently pursuing the Ph.D. degree in Department of Electrical Engineering and Electronics at University of Liverpool. His research interests include fault-tolerant operation and control of power electronic converters in doubly-fed induction machines.

Jikai Si was born in Henan Province, China, in 1973. He received the B.Eng. and M. Eng. degrees from Jiaozuo Institute and Technology, Henan Polytechnic University, Jiaozuo, China, in 1998 and 2005, respectively. He received the Ph.D. degree in The School of Information and Electrical Engineering at China University of Mining and Technology, Xuzhou, China. Currently, he is a Professor in the Henan Polytechnic University. His main research interests include the theory, application and control of special motor.